PHILOSOPHICAL TRANSACTIONS OF THE ROYAL SOCIETY B BIOLOGICAL SCIENCES

The vortex wake of a 'hovering' model hawkmoth

Coen Van den berg and Charles P. Ellington

Phil. Trans. R. Soc. Lond. B 1997 **352**, 317-328
doi: 10.1098/rstb.1997.0023

The vortex wake of a 'hovering' model hawkmoth

COEN VAN DEN BERG* AND CHARLES P. ELLINGTON

Department of Zoology, University of Cambridge, Downing Street, Cambridge CB2 3EJ, UK

CONTENTS

SUMMARY

Visualization experiments with *Manduca sexta* have revealed the presence of a leading-edge vortex and a highly three-dimensional flow pattern. To further investigate this important discovery, a scaled-up robotic insect was built (the 'flapper') which could mimic the complex movements of the wings of a hovering hawkmoth. Smoke released from the leading edge of the flapper wing revealed a small but strong leading-edge vortex on the downstroke. This vortex had a high axial flow velocity and was stable, separating from the wing at approximately 75% of the wing length. It connected to a large, tangled tip vortex, extending back to a combined stopping and starting vortex from pronation. At the end of the downstroke, the wake could be approximated as one vortex ring per wing. Based on the size and velocity of the vortex rings, the mean lift force during the downstroke was estimated to be about 1.5 times the body weight of a hawkmoth, confirming that the downstroke is the main provider of lift force.

1. INTRODUCTION

Over the past decade it has become increasingly clear that a quasi-steady aerodynamic explanation of insect flight cannot account for the high lift produced by their wings: unsteady lift-enhancing mechanisms must also be involved (for reviews see Ellington 1995; Willmott *et al*. 1997). A number of high-lift mechanisms have been proposed (Weis-Fogh 1973; Nachtigall 1979; Ellington 1980, 1984*a*) which, at the Reynolds numbers appropriate to insect flight, should produce a large leading-edge vortex. The swirl around the leading edge enhances the circulation and hence the lift, but the vortex should be unstable for two-dimensional (2D) wing motions: it should break away after a few chords of travel, leading to a deep stall with complete loss of lift. Two-dimensional model experiments on the aerodynamic mechanisms have indeed confirmed the presence of a large leading-edge vortex which subsequently breaks away (Maxworthy 1979; Savage *et al*. 1979; Spedding & Maxworthy 1986; Dickinson & Götz 1993; Sunada *et al*. 1993; Dickinson 1994).

However, evidence for the leading-edge vortex is contradictory in flow visualization experiments with real insects (Brodsky & Grodnitsky 1985; Brodsky 1991; Grodnitsky & Morozov 1992, 1993). Recently, detailed visualization of hawkmoth (*Manduca sexta*) flight did reveal a clear leading-edge vortex (Willmott *et al*. 1997), but at low flight speeds it was much smaller than in the 2D model experiments. Using stereophotography, Willmott *et al*. (1997) also discovered that the flow was strongly three-dimensional (3D) with

* Current address: Faculty of Human Movement Sciences, Vrije Universiteit, Van der Boechorststraat 9, 1081 BT, Amsterdam, The Netherlands.

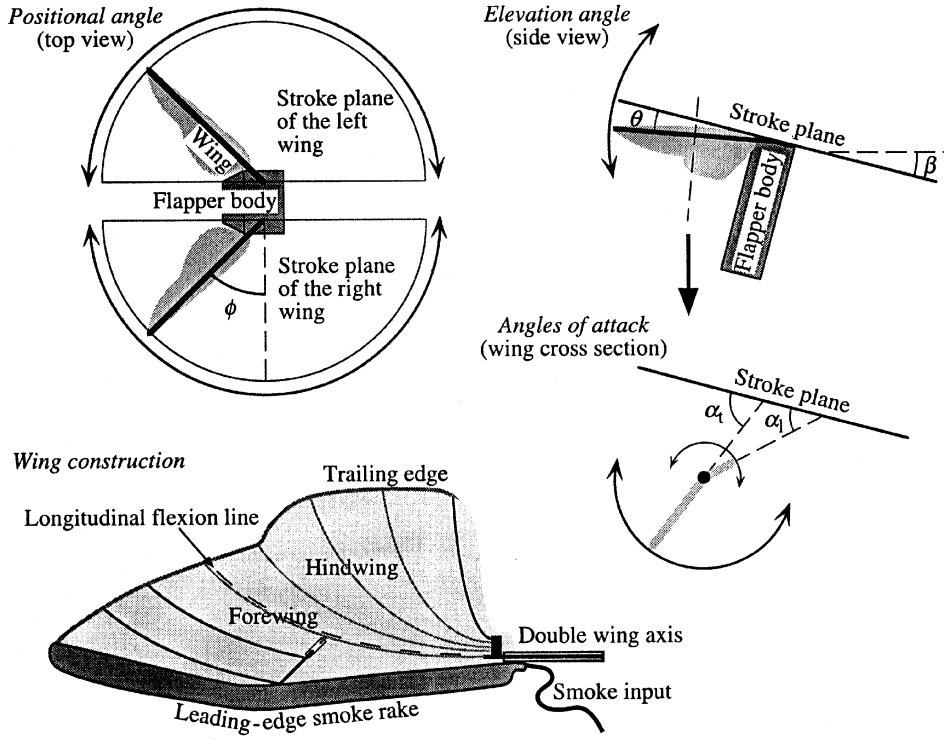

Figure 1. Schemes of the degrees of freedom and the construction of the flapper wing. The flapper is shown in the orientation of a hovering hawkmoth, with a stroke plane angle of 15°. The arrows show the maximal range of movement for each degree of freedom. Note that α_l and α_t are measured with respect to the stroke plane. Abbreviations: $\alpha_{l,t}$ is the angle of attack of the leading-edge/trailing-edge sections; β is the stroke plane angle; θ is the elevation angle, perpendicular to the stroke plane; ϕ is the positional angle, in the stroke plane.

a substantial spanwise velocity component. Previous visualization studies of insects have largely ignored three-dimensional effects and, by definition, 2D model experiments cannot show any 3D character of the flow. Such models lack the spanwise velocity gradient which is present during flapping flight. This gradient is most pronounced during hovering, where the velocity increases linearly from zero at the wing base to a maximum at the wing tip. The velocity gradient might result in a spanwise pressure gradient with a significant spanwise flow component along the wing. Maxworthy (1979) found such a spanwise flow for his 3D model of the 'fling' motion, but Saharon & Luttges (1987, 1988) did not in their 3D visualization experiments on a dragonfly model.

The results of Willmott *et al.* (1997) contain a number of interesting features: the small leading-edge vortex, a spanwise flow along the wing, a somewhat larger than expected tip vortex, and evidence for separate shedding of stopping and starting vorticity at the ends of the wingbeat. However, there are inherent limitations in such experiments: the position of vortices can only be inferred indirectly from smoke flowing around them, so detailed measurements are impossible. Furthermore, flow velocities in the wake cannot be estimated. To investigate these aspects of the flow in more detail, we therefore built a 3D mechanical model that mimics the wing movements of the *Manduca* much more closely than 2D models. This 'flapper' allowed visualization by releasing smoke from the leading edge of the wing, right into the core of the leading-edge vortex. The wingbeat frequency of the flapper was scaled to ensure aerodynamic similarity with the hawkmoth. In this paper, a detailed description is given of the wake produced by the model while mimicking a hovering *Manduca*; furthermore, the mean lift force during the downstroke is estimated from the flow velocity in the wake. Details of the dimensions, stability, circulation and lift of the leading-edge vortex are given in a companion paper (Van den Berg & Ellington 1997). In these studies we concentrated on the downstroke, which was shown to be far more active than the upstroke by Willmott *et al.* (1997). The complicated 3D wing movements also did not allow simultaneous analysis of the downstroke and the upstroke.

2. MATERIALS AND METHODS

(*a*) *The flapper*

A robotic insect (the 'flapper') was built to mimic the movements of insect wings during flapping flight. It consists of a body and two wings, mounted on a stand (figure 1; see also figure 3*a*, *b*). The flapper body houses four d.c. servo motors (RS 336–292) and an elaborate gearbox to drive the wing movements. Since the hawkmoth is a functionally two-winged insect, its fore- and hindwing are represented as one wing. The movements of the left and right wings are mechanically coupled, and each is driven by four coaxial shafts that engage with the motors via spur gears. The outer shaft turns a yoke at the wing base, supplying a flapping motion in the stroke plane. The next shaft elevates the wing within the yoke, via two bevel gears, providing

movement perpendicular to the stroke plane. The two inner shafts are coupled, again via bevel gears, to coaxial shafts at the wing base. The fore- and hindwing sections of each wing are mounted on these coaxial shafts and can twist independently. Hence, four rotational axes go through one point at the wing base, i.e. the wings have four degrees of freedom (figure 1): (i) the *positional angle*, ϕ, allowing 180° flapping of the wing in the stroke plane; (ii) the *elevation angle*, θ, allowing 30° movement of the wing on either side of the stroke plane; (iii) the *angle of attack of the leading-edge section*, α_l, allowing 180° rotation of the leading-edge section with respect to the stroke plane and (iv) the *angle of attack of the trailing-edge section*, α_t, allowing 180° rotation of the trailing-edge section with respect to the stroke plane. The leading-edge and trailing-edge sections of the flapper wing do not correspond exactly to the anatomical fore- and hindwings of the hawkmoth; the wings of the flapper and the hawkmoth flex mainly about the longitudinal flexion line (figure 1), which lies within the forewing. Note also that the angles of attack are measured relative to the stroke plane (figure 1), not relative to the wing-tip path or to the relative wind.

With these degrees of freedom and a suitable model wing (see below), the flapper can accurately mimic most aspects of the wing movements of the hawkmoth, including spanwise changes in twist, camber and flexion. Some spanwise bending of hawkmoth wings does occur during pronation and supination (Willmott 1995), but this feature has not been incorporated.

The torque exerted on each wing base by the weight of the wing was reduced by a lead counterweight and an adjustable anti-backlash spring for the long gear train. The angle-of-attack axes were connected by a clock spring, which removed backlash on both axes. The torque of the hindwing weight was cancelled about its axis with a counterweight at the wing base.

The flapper was mounted on a 1 m high heavy stand. The stroke plane angle of the wings with respect to the gearbox mechanism was fixed at 90°. The flapper body was tilted 23° 'head-up' with respect to the horizontal to reduce the backlash problem in the elevation and the positional angle drives. During image analysis, however, the images were rotated to the hovering position of *M. sexta*, with a stroke plane angle, β, of 15° (Willmott 1995).

(*b*) *The flapper wings*

The flapper's wings are approximately ten times larger than *Manduca*'s, and they were designed by Dr R. J. Wootton. The wings are 46.5 cm long, have a surface area of 513 cm^2 and weigh 189 g. The maximum wing thickness is 0.34 cm. The shape of the wings was copied from a tracing of the outline of a coupled fore- and hindwing of *M. sexta*. The wing bases of the flapper are separated by 10 cm. The ratio of wing-base separation to wing length is 1:4.7; in *M. sexta* this ratio is approximately 1:5. To avoid interference with the gearbox the wing area started at 6 cm from the wing base, creating a gap between the wing base and the flapper body. Air is likely to leak through such a gap, from the functional underside of the wing to the top side. In contrast, the hawkmoth wing area starts immediately at the wing base, and the gap between wings and body is tightly closed.

The wings consist of a frame of brass tubes (thickness 0.235 cm), covered on both sides with black, elastic cloth (a Jersey knit). The main support for the forewing is a stiff, brass smoke rake (see below) extending along its length (figure 1). From halfway along its length two tubes radiate towards the trailing edge of the forewing, reinforcing the tip region of the wing. The base of the leading-edge smoke rake is connected to the forewing axis of the gearbox. From the wing base, five curved brass tubes radiate towards the trailing edge. The most basal one is fixed to the hindwing axis, while the other four are free to rotate in their sockets, which are aligned on a piece of brass, which is connected to the hindwing axis (coaxial with the forewing axis). All struts are connected by a flexible trailing edge. To allow a gradual twist of the trailing edge, the tips of the struts must be able to rotate relative to it; end pieces were mounted on the tip of each strut to allow such rotations. Halfway along the wing length, the anterior and posterior regions of the wing are loosely connected using a piece of flexible tubing, to simulate the longitudinal flexion line of the forewing (figure 1). As a result of this construction, the leading edge and wing-tip region remain relatively stiff when the wing is cambered, but the trailing edge bends smoothly from base to tip with a more pronounced curvature around the flexion line. The resulting wing deformations mimic quite accurately those of hawkmoth wings during hovering flight (Willmott 1995).

The wing cloth was pre-stretched on a wooden frame, glued (using Bostik all-purpose glue) to both sides of the wing frame and trimmed to fit the exact wing shape. The pre-stretched cloth did not wrinkle on the concave side of the wing when it was cambered. The cloth exerts strong elastic forces on the angle-of-attack servos when the wing is cambered, and these were cancelled by a bistable spring.

(*c*) *The leading-edge smoke rake*

A smoke rake was designed which can emit smoke evenly and at low speed (less than 5 cm s^{-1}) along the length of the leading edge. The smoke used for flow visualization was an oil vapour, produced with an FVSP/E smoke generator (Nutem Ltd) and a medicinal white oil (Shell Ondina EL). The smoke rake is 2 cm wide with a long strip of envelope stiffener (Challoner Mktg Ltd) sandwiched between brass foil (thickness 0.013 cm), cut to the shape of the leading edge. The channel construction of the stiffener provided parallel paths, approximately perpendicular to the leading edge, for smoke release; sections of the rake could be closed off by wedging in strips of reticulated foam covered with tape. The rake is closed at its inner edge by a brass tube (0.32 cm outer diameter) connected to the smoke generator at its base, with holes in its wall which gradually become larger and more closely spaced towards the wing tip (from 0.1 cm diameter at an 8 cm interval to 0.2 cm diameter at

1 cm intervals). This design ensures a fairly even release of smoke over the length of the rake. Over the basal three-quarters of the wing, 0.5 cm wide strips of reticulated foam were wedged against the tube to reduce the speed of the smoke.

The released smoke visualizes streaklines, not streamlines or particle lines. For a study of the near wake, however, the differences between streak- and streamlines will be minor (Gursul *et al*. 1990). Smoke emitted from the leading-edge smoke rake when the flapper was motionless reached speeds of 3–7 cm s^{-1}, due to air movements in the experimental room. These air currents are small relative to the flow velocities during flapping, which are in the range of 25–50 cm s^{-1}.

(*d*) *Wing movement*

The wing movements of the flapper were controlled by a Macintosh Quadra 650 computer with D-A converters (NB-AO6, National Instruments) for analogue inputs to the servos. Customized software was written in LabView 3.0.

The movements were based on detailed measurements of the wing kinematics of a hovering hawkmoth, *M. sexta*, in one high-speed video sequence (Willmott 1995). The hawkmoth was a male with a body mass of 1.58 g, a wing length of 4.85 cm and a wingbeat frequency of 26.1 s^{-1}. For aerodynamic similarity, the flapper had to operate at the same Reynolds number, *Re*, as the hawkmoth. The flapping velocity is proportional to ΦfR, so an appropriate *Re* is defined by

$$Re = \frac{\Phi \cdot f \cdot R^2}{\nu},$$

where Φ is wingbeat amplitude, f is frequency, R is wing length and ν is kinematic viscosity. The wing length of the flapper is 9.6 times that of the hawkmoth, so f had to be decreased to 0.28 s^{-1} to keep *Re* constant. A wingbeat frequency of 0.30 s^{-1} was therefore used in all experiments. This low frequency for the scaled-up model has the added advantage that conventional video is adequate to record the flow patterns. Note further that the air velocities (in cm s^{-1}) will be a factor of 9.6 *lower* for the flapper than the hawkmoth. It must be emphasized that the aerodynamic forces (proportional to f^2R^4) will be unchanged; the flapper should produce the same lift as the hawkmoth.

A flat plate at high angle of attack freely sheds vortices at a certain frequency, f_{vs}. Similar vortex shedding may occur with the flapper and it is important to ensure that the timing of free vortex shedding relative to the forced vortex shedding of a wingbeat is not altered. The relevant scaling parameter is the Strouhal number, *St*: the product of f_{vs} and the chord divided by the velocity. For a flapping wing in still air the velocity is proportional to ΦfR, so *St* is proportional to f_{vs}/f. However, *St* is also constant for a given *Re* (e.g. Dickinson 1994), which shows that the relative frequencies of free and forced shedding should be the same for the flapper and the hawkmoth.

Willmott (1995) measured the positional angle, elevation angle and the average angles of attack for the basal and distal halves of the wings of the hovering hawkmoth. He found that the first three terms of a Fourier series approximated each data set very satisfactorily, and these smoothed records were used as input functions for the flapper kinematics.

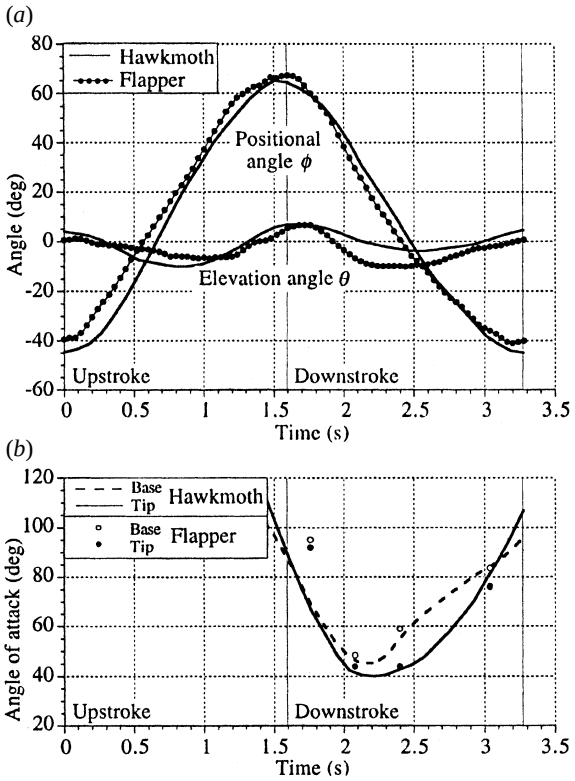

Figure 2. The kinematics of the flapper compared with a hovering hawkmoth, *Manduca sexta*. (*a*) The positional angle, ϕ, and the elevation angle, θ. (*b*) The angles of attack during the downstroke. The angles of attack of the wing base and tip of the flapper were recalculated using Willmott's method. The dotted line and open symbols represent the wing base, the continuous line and filled symbols represent the wing tip. Data for *M. sexta* are from Willmott (1995).

To check the performance of the flapper, its movements were compared with the kinematic data of Willmott (1995). The flapper wing movements were measured by tracing the wing tip in a side view and a frontal view of the flapper. The movements proved to depend on the tension in the adjustable anti-backlash spring, but at a particular spring tension (i.e. during the experiments), they were very repeatable. Because of the tension setting, the positional angle ranged between −40 and 51° during the flow visualization experiments, whereas during the flapper kinematics experiments it ranged between −40 and 61° (figure 2*a*). Apart from this difference, the positional angle of the flapper wing corresponded quite well with the hawkmoth data (figure 2*a*). The elevation angle also agreed with the hawkmoth data in the overall pattern of the movement, but during the mid-downstroke the angle was too low by up to 10°.

The angles of attack were measured in the video sequences which were made for analysis of the leading-edge vortex (see below). Hence, these angles were only obtained at four positions during the downstroke; the

same camera positions were not suitable for analysis of the upstroke, because the elevation angles were different. Willmott (1995) measured spanwise values of the angle of attack for a line connecting the leading and trailing edges of the wing, and then calculated mean values for the base and tip regions. We measured the angle of attack of the leading-edge and trailing-edge sections of the wing, corresponding to rotation of the angle-of-attack axes of the wing. Due to the wing's construction, these methods are quite similar; the angle of attack at the wing tip is exclusively due to the leading-edge section, whereas at the base it is dominated by the much wider trailing-edge section. However, to allow accurate comparison with Willmott's data, we recalculated the angles of attack of the flapper for figure 2*b*, using Willmott's method. The angle of attack correspondence was good (figure 2*b*), with differences of less than 10°, except just after pronation. This is because the maximum positional angle only reached 51° during the flow visualization experiments, instead of 61° (see above), which introduces an apparent phase lag; the angles of attack at $\phi = 50°$ do correspond very well with those during late pronation.

The kinematic differences noted here may have some effect on the supination and pronation phases, but less so on the downstroke and upstroke phases of the wingbeat. The flow phenomena described in this paper are fairly insensitive to the precise wing kinematics, as observed in earlier experiments with the flapper (see figure 8 in Van den Berg & Ellington 1997).

(*e*) *Filming and analysis*

The dimensions of the experimental room (9 m × 6.5 m × 5 m) were five to nine times the wingspan of the flapper. In their analysis of vortex wakes in a confined volume, Rayner & Thomas (1991) suggest that wall effects are significant in enclosed volumes of up to three times the wing span. Hence, wall effects can be ignored here.

The flapper was filmed with a Hitachi CCTV video camera (WV-BL600/B), with a Fujinon zoom lens (1.2/12.5–75) and a Panasonic NV-J35B video recorder. Most video recordings used for analysis employed a 'light slice' to illuminate a cross-section of the flow. The camera was positioned such that, at a particular positional angle of the wing, the wing axis was exactly perpendicular to the image plane. The spanwise position of interest was lit by an Arri 'junior' 1000 W manual spotlight with almost closed barn doors, giving a slit of light approximately 7 cm wide and parallel to the image plane of the camera. Flow cross-sections were recorded at four positional angles ($\phi = 50$, 30, 0 and $-36°$) and, for each positional angle, at up to five spanwise positions (0.25*R*, 0.50*R*, 0.63*R*, 0.75*R* and 0.87*R*, where *R* is wing length). At each of these cross-sections, flow near the leading edge was recorded at higher magnification as well as an overall view of the wake at lower magnification. Details of the leading-edge visualization results are reported elsewhere (Van den Berg & Ellington 1997).

Although most smoke spiralled into the leading-edge vortex towards the tip vortex, enough smoke was present around the wing to trace the movement of the downstroke starting vortex, which combines with the stopping vortex of the preceding upstroke to form the starting/stopping vortex (SS vortex). Up to ten downstrokes were selected to measure the position of the centre of this vortex during the downstroke. The direction of the vortex movement and the 95% confidence intervals of that direction were calculated using linear regression of the combined data of all analysed downstrokes for each measurement site.

As explained above, the light slice was always perpendicular to the wing axis. The angle β between the stroke plane and the horizontal is 15°, and hence flow cross-sections are slightly tilted with respect to the vertical. This tilt equals β multiplied by sin (ϕ), or 11.5° at $\phi = 50°$, 7.5° at $\phi = 30°$, 0° at $\phi = 0°$ and 8.8° at $\phi = -36°$. These fairly small tilt angles were ignored in the analysis.

3. RESULTS

A high quality of flow visualization of the wake was achieved with the flapper. Since smoke was released from the leading edge the vortex cores were marked by smoke, whereas in visualization experiments with insects only the flow around the vortices is visualized. The flapper, therefore, allowed a more detailed analysis of the wake structure and especially of the leading-edge vortex (Van den Berg & Ellington 1997) than has been possible before. Due to destructive interactions of merging vortex structures (see below), most of the vortices in the wake are rather tangled, with a broken-down core of unclear diameter. The leading-edge vortex was the only well-behaved flow structure with clear smoke streaklines showing details of its shape.

(*a*) *The leading-edge and tip vortices*

The flow visualization experiments revealed a rather small but strong leading-edge vortex during the downstroke (figure 3). The most surprising feature of this vortex was its large axial velocity component (figure 4*b*, *c*): the maximum axial velocities equalled the mean velocity of the wing tip (about 50 cm s^{-1}; Van den Berg & Ellington 1997). Throughout the downstroke, the leading-edge vortex was attached to the wing surface. Two dividing stream surfaces (one on the lower surface of the wing and one on the upper surface) separated the free flow around the wing from that rolling up into the leading-edge vortex (figures 4, 3*c* (upper surface only)). The leading-edge vortex is not strictly a trapped vortex, but is rather a rolled-up vortex sheet (Wu *et al.* 1991; Délery 1994). Due to the continuous roll-up of air into the vortex, its diameter rapidly increased from wing base to tip (figure 3*c–f*). The free flow close to the leading-edge vortex will also exhibit a strong spanwise flow (figure 4*d*), which was very clear in flow visualization experiments with near-

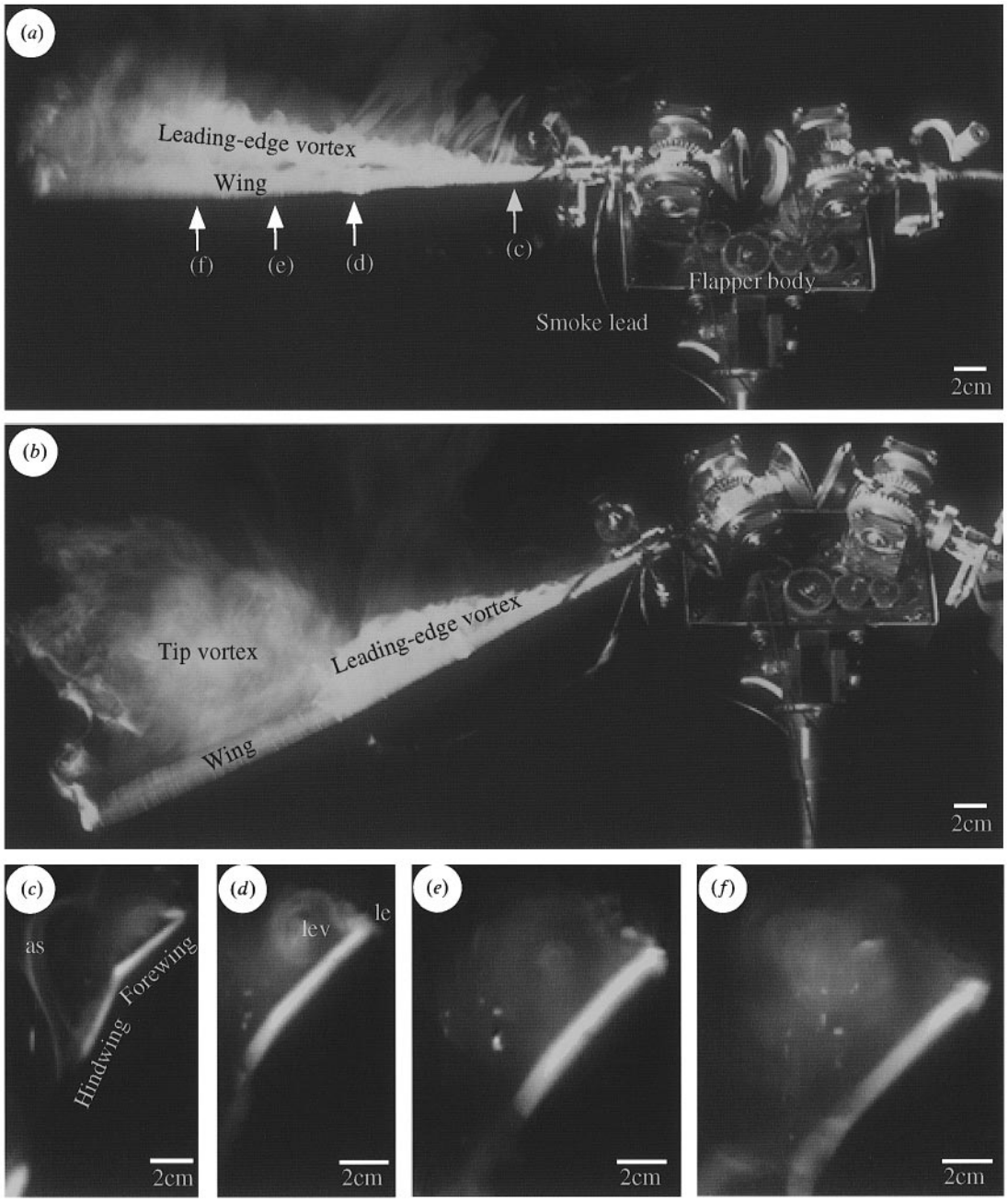

Figure 3. Flow visualization of the leading-edge vortex during the downstroke. Smoke was released from the leading edge of the right wing. (*a*) The leading-edge vortex at $\phi = 0°$, viewed parallel to the wing surface, which approximately corresponds to a top view of a hovering hawkmoth. In this image, some of the mechanical components of the flapper can be seen. Note the slight motion blur of the wing, especially towards the tip. The positions of the cross-sections shown in (*c*)–(*f*) are indicated. (*b*) The leading-edge vortex at $\phi \approx -25°$. The development of a large tip vortex, with a broken-down core, at approximately three-quarters of the wing length is very clear in this image. (*c*)–(*f*) Cross-sections of the leading-edge vortex (lev) at $0.25R$, $0.50R$, $0.63R$ and $0.75R$. In this spanwise series, the diameter of the vortex increases; towards the wing tip it separates and becomes less distinct as it blends into the tip vortex. Note the attachment streakline (as) in (*c*), which shows in cross-section the upper dividing stream surface of figure 4 (*c*) and (*d*).

hovering hawkmoths (Willmott *et al.* 1997). The forward speed during 'near-hovering' was 40 cm s^{-1}, which is very close to hovering: the insect advances by less than its mean wing chord during each wingbeat. A similar but smaller leading-edge vortex was present during the upstroke. A full analysis of the downstroke leading-edge vortex is given in a separate paper (Van den Berg & Ellington 1997).

As the leading-edge vortex spiralled towards the wing tip its core became unstable and, at approximately $0.75R$, it detached from the wing surface. Here, the vortex broke down and connected to a tangled tip vortex with a broken-down vortex core (figure 3*b*). During the downstroke the tip vortex became very large, covering the outer quarter of the wing. As the wing swept through the air, the leading-edge vortex fed vorticity into the tip vortex, thus gradually building up a vortex ring in its wake (figure 4*c*, *d*).

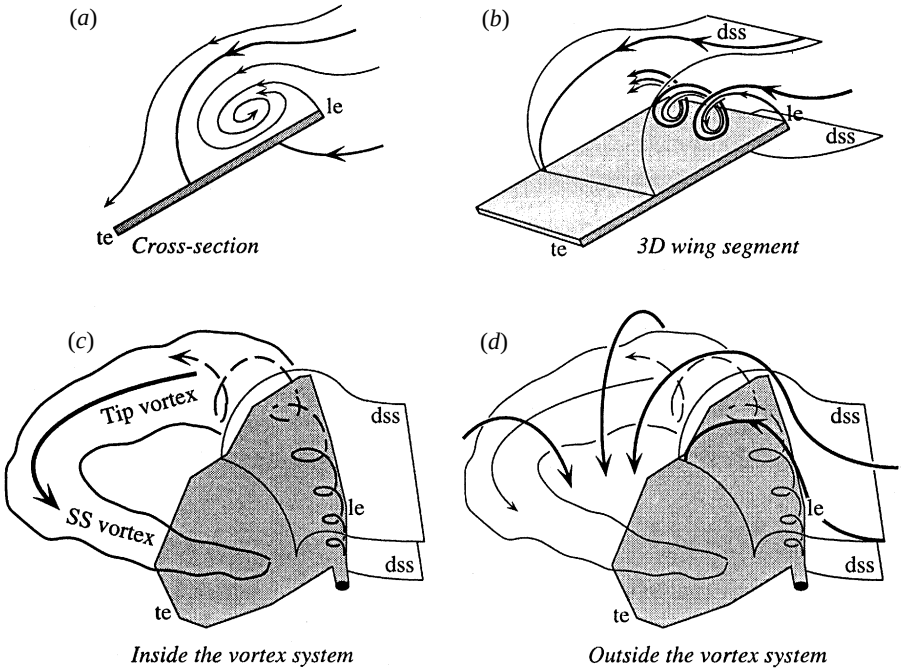

Figure 4. Flow patterns in the wake. (*a*) Cross-section of the leading-edge vortex, comparable to figure 3 (*c*)–(*f*). Bold lines indicate the dividing streamlines. (*b*) Three-dimensional segment of the leading-edge vortex, showing the axial flow component. Streamlines roll up into the vortex as it spirals towards the wing tip (into the paper). (*c*) The flow between the two dividing stream surfaces (i.e. the flow inside the vortex system). The vortex wake of the flapper is shown halfway during the downstroke. The growth of the tip vortex is fed by the axial flow of the leading-edge vortex. (*d*) The flow outside the dividing stream surfaces. There is a high downwash velocity in the centre of the vortex ring created by the wing. Note that the flow directly above the leading-edge vortex has a strong spanwise component. Abbreviations: le, leading edge; te, trailing edge; dss, dividing stream surface; SS vortex, combined starting/stopping vortex.

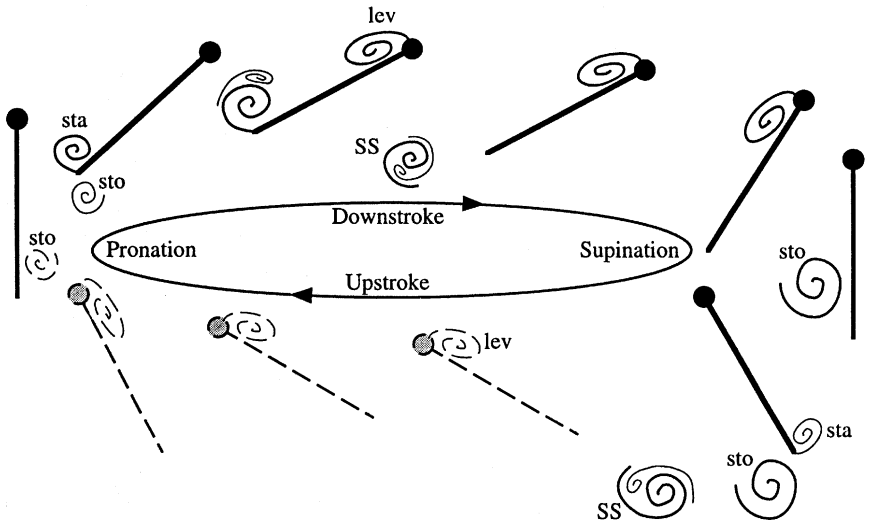

Figure 5. The formation and roll-up of starting (sta) and stopping (sto) vortices during a complete wingbeat cycle. The four main stages of the wingbeat are indicated in the centre, the loop signifying the wingbeat cycle. The greater part of the upstroke is indicated by dashed lines, since it was not observed directly. The leading edge of the wing is indicated by a black circle. The relative wing positions are not to scale. Abbreviations: sta, starting vortex; sto, stopping vortex; lev, leading-edge vortex; SS, combined starting and stopping vortex.

(*b*) *The starting/stopping vortex*

At the end of the upstroke a stopping vortex was shed. During early pronation this vortex was hidden behind the wing in the video recordings, but during late pronation (just prior to the downstroke) it appeared from behind the wing and rolled over the trailing edge (figure 5). Meanwhile, the downstroke started and a starting vortex was generated and shed from the trailing edge, rolling up on the anatomical topside of the wing. The downstroke starting vortex was much stronger than the upstroke stopping vortex, which spiralled towards the starting vortex and amalgamated with it. The combined SS vortex had a

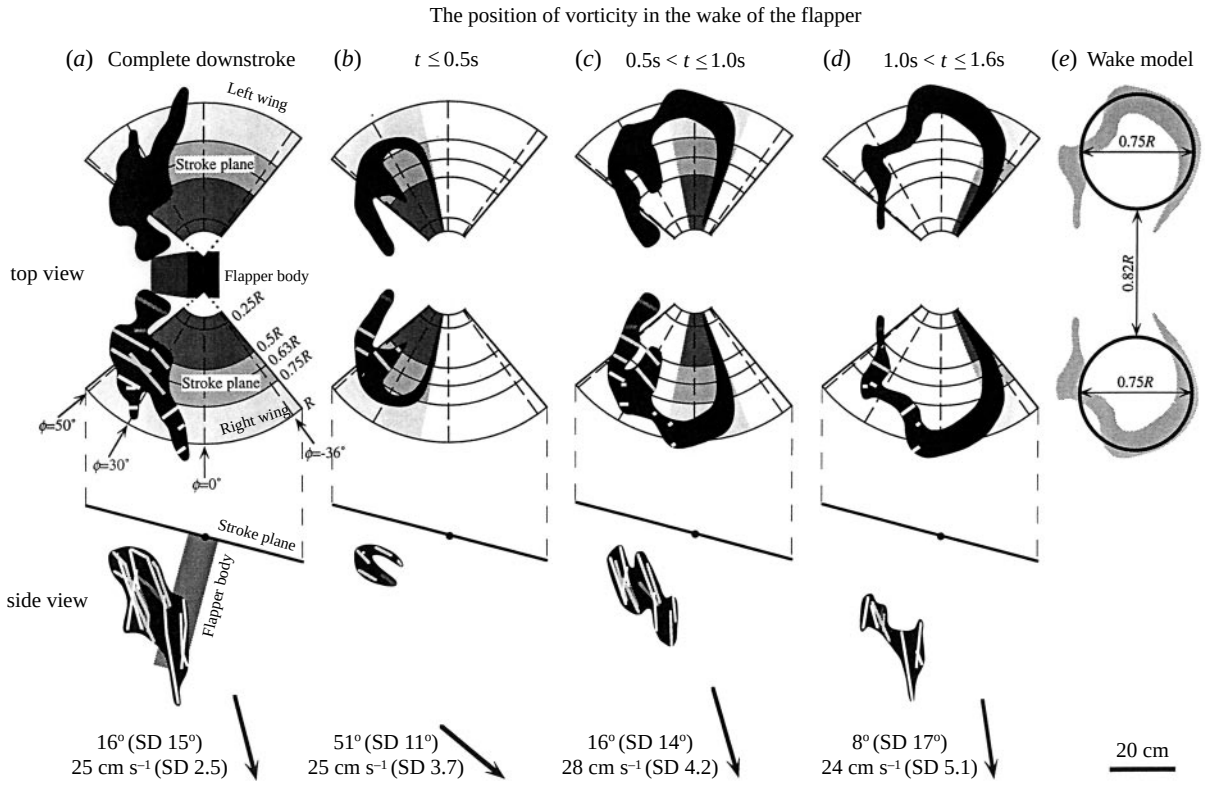

Figure 6. Reconstruction of the approximate shape and movement of the vortex wake by tracking the centre of the downstroke vortex (SS vortex and early tip vortex). The reconstructions are shown in the orientation of the hovering hawkmoth. A top view of the reconstructed wake is shown in the upper half of each panel and corresponding side views in the lower halves. The vorticity shed during the complete downstroke (1.6 s) is shown in (*a*), while (*b*)–(*d*) show both the shed and the leading-edge vorticity during three subsequent, shorter, time spans; (*b*) shows the first 0.5 s, (*c*) the second 0.5 s and (*d*) the remainder of the downstroke (approximately 0.6 s). *Top views*. The area swept by the wing axis is shown as a shaded segment of a circle. Note that the plane of these top views is not exactly parallel to the stroke plane (the stroke plane angle is 15°). The four camera axes are indicated by dashed radius lines; the spanwise positions where the measurements were taken are also indicated. On the top view of the right wing, the (projected) trajectories of all the downstroke vortex measurements are shown as lines. These lines are drawn at the middle of the light slice, which was 7 cm wide. Three spanwise segments within the wake are distinguished by their greyness: darkest for $0 < r \leqslant 0.50R$, intermediate for $0.50R < r \leqslant 0.75R$ and lightest for $0.75R < r$, where r is the spanwise position as a fraction of the wing length, R. This shading code is also used for the (projected) trajectories. The shape of the vortex wake was estimated from the position of the trajectories and is indicated as a black area. This shape was mirrored onto the top view of the left wing. In the three 0.5 s reconstructions (*b*)–(*d*), the approximate positions of the leading-edge vortex and the tip vortex were added to the black area, thus showing the approximate shape of the developing wake. The wake shape at the end of the downstroke (*d*, top view) is repeated in (*e*) for comparison with a model of the wake as two adjacent vortex rings of diameter $0.75R$ separated by a distance of $0.83R$. *Side views*. The trajectories of the centre of the downstroke vortex are shown with respect to the stroke plane. The greyness of the trajectories corresponds to the spanwise positions indicated in the top views. The mean forward angle and velocity of the trajectories are given as a vector and in words (mean and standard deviation).

broken-down vortex core. During the downstroke, the tip vortex connected to the SS vortex and the wake grew (figure 4*c*). At the end of the downstroke a strong stopping vortex was shed (figure 5) and the downstroke vortex wake disconnected from the wing surface. At the start of the upstroke, a weak starting vortex was observed which spiralled towards and merged with the downstroke stopping vortex, creating another combined SS vortex.

This suggests that the strong vortex rings of the downstroke are connected by weak upstroke vortex rings, thus forming a chain of alternating weak and strong vortex rings. This agrees with flow visualization results for the hawkmoth during near-hovering (Willmott *et al*. 1997), but we have not studied the upstroke wake in sufficient detail to elaborate.

(*c*) *The downwash velocity and shape of the wake*

As there is no clear distinction between the SS vortex and the tip vortex (they are part of a continuous vortex ring, see figure 4*c*, *d*), we will refer to them as the 'downstroke vortex'. The position of the centre of the downstroke vortex could be estimated quite accurately, but not its diameter. The shape of the vortex wake with respect to the stroke plane, as shown in top views in figure 6*a–d*, could therefore be reconstructed by tracking the centre of the downstroke vortex during several downstrokes. The mean forward and downward movements of the vortex centres are shown in the side views of figure 6*a–d*.

During the complete downstroke, the downstroke vortex was concentrated in the rearmost half of the

Table 1. *The movement of the centre of the downstroke vortex (SS vortex and early tip vortex) during three downstroke time intervals as a function of spanwise position,* r ; *vortex trajectories are shown in figure 6. The forward angle is measured with respect to the vertical. The forward angle and the velocity are given for a plane parallel to the symmetry plane of the flapper; movement perpendicular to this plane was ignored. Mean values and standard deviations (where appropriate) are given. The number of observations is given in parentheses*

	$t \leqslant 0.5$ s	$0.5\text{ s} < t \leqslant 1.0$ s	$t > 1.0$ s
forward angle (deg)			
$r < 0.50R$	54 (1)	28±10 (3)	8±31 (2)
$0.50R < r \leqslant 0.75R$	51±13 (4)	24±8 (4)	10±21 (2)
$r > 0.75R$	(0)	5±9 (6)	7±14 (5)
velocity (cm s^{-1})			
$r < 0.50R$	24.2 (1)	27.4±5.1 (3)	28.8±4.2 (2)
$0.50R < r \leqslant 0.75R$	25.1±4.2 (4)	27.6±5.1 (4)	21.1±8.5 (2)
$r > 0.75R$	(0)	28.3±3.9 (6)	22.9±3.5 (5)

swept area (figure 6*a*). Its centre (in a plane parallel to the symmetry plane of the flapper) moved 16° forward with respect to the vertical with a mean velocity of 25 cm s^{-1}. We subdivided the downstroke into three periods of 0.5 s each (figure 6*b–d*).

During the first 0.5 s of the downstroke (figure 6*b*), the mean velocity of the downstroke vortex centre was 25 cm s^{-1} in a direction tilted 51° forward with respect to the vertical (table 1). This initial movement was strongly influenced by the trailing edge, which was moving roughly parallel to the stroke plane, i.e. tilted 75° forward with respect to the vertical: the downstroke vortex had not yet been fully shed. Depending on the experiment, the SS vortex was observed at one of two positions (figure 6*b*, *c*). These positions probably correspond to the starting and stopping vortices, which had not yet fully merged.

In the interval $0.5\text{ s} < t < 1.0$ s, the vortex wake moved slightly forward and radially outward (figure 6*c*). The average direction of the vortex centre was 16° forward, indicating that the vortex had now been shed. Its mean velocity was 28 cm s^{-1} (table 1).

Between $t = 1.0$ s and the end of the downstroke ($t \approx 1.6$ s) the vortex wake moved farther forward and outward, even extending outside the swept area (figure 6*d*). The average movement of the vortex centre was 8° forward and the mean velocity was 24 cm s^{-1} (table 1). The final velocity of the centre of the starting vortex was slightly lower and more nearly vertical than in the previous period, although this difference was not significant. The corresponding net aerodynamic force exerted on the wing therefore presumably points upwards and slightly backwards, as is to be expected during the downstroke.

The velocity of the centre of the SS vortex was not strongly dependent on spanwise position or on the stage of the downstroke (table 1). The velocity was fairly constant, ranging from 21 to 29 cm s^{-1}. The forward angle of the movement was dependent on the time since the start of the downstroke (table 1), as noted earlier (figure 6*b–d*, side views). This forward angle did not vary along the wing span, except when $0.5\text{ s} < t < 1.0$ s, where it was more vertical near the wing tip. Presumably, shedding of the SS vortex was completed earlier at the narrow wing tip, and the downward path of its centre was established more quickly. Note further that the wing tip moved at higher velocity than the wing base; therefore, even if the spanwise wing chord were constant, the wing tip would travel more chord lengths in the same length of time than the wing base, leading to quicker vortex shedding at the tip.

Proximally, the vortex wake (figure 4*c*) might well be closed by a short root vortex, producing one (distorted) vortex ring per wing. The root vortex will be short due to the limited wing movements at the wing base. The shape of the downstroke vortex wake suggests that this is the case (figure 6*e*). Video images of the wake, viewed in various planes perpendicular to the stroke plane, show a clear root vortex, confirming that there is indeed one vortex ring per wing. These rings slowly move away from each other over the course of time (figure 6*b–d*, top views).

4. DISCUSSION

The flow visualization results obtained with the scaled-up flapper are in excellent agreement with the visualization results for *Manduca* (Willmott *et al.* 1997). At (near) hovering speeds the downstroke wake can be described for both flapper and hawkmoth as follows: a small leading-edge vortex is generated, with a strong axial flow component increasing in diameter from wing base to tip, separating from the wing at approximately $0.75R$ during the latter half of the downstroke, and merging with a large tip vortex with broken-down core, which connects to a combined SS vortex. The only significant difference between the flapper and *Manduca* is the absence of a root vortex in *Manduca*, but this can be readily explained (see below). The excellent agreement confirms that the flapper is a valid and powerful tool for studying details of the aerodynamics of hovering flight.

(*a*) *The leading-edge vortex*

A leading-edge vortex was found with a much smaller diameter than that predicted from experiments using linearly translating wings (Savage *et al.* 1979; Dickinson & Götz 1993). It seems that the flapping motion of the wing triggered a 3D development of the flow; a strong axial flow was established, resulting in increased stability of the vortex and a decrease of its

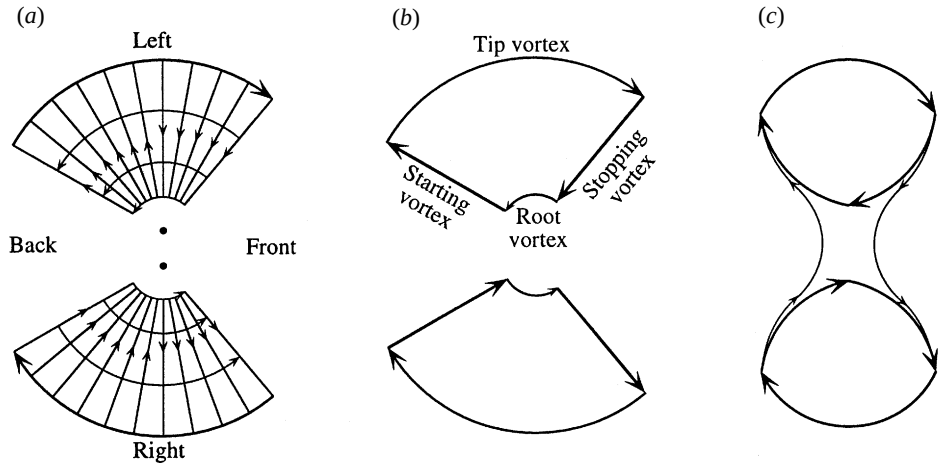

Figure 7. Development of the vortex wake during the downstroke of a hovering insect. (*a*) Initially, a vortex sheet will be shed from each wing, as the circulation changes during the downstroke and along the span. (*b*) The vortex sheets are unstable and will quickly roll up into one wedge-shaped vortex 'ring' per wing, consisting of a starting vortex, a tip vortex, a root vortex and a stopping vortex. (*c*) The wake is likely to evolve into two adjacent, circular vortex rings. If the root vortices cancel, these rings may connect in a single dumbbell-shaped vortex structure.

diameter. Similarly, the diameter of the vortex in Maxworthy's (1979) 3D fling experiment seemed much smaller than that in his experiments with translating wings, which were described in the same paper. In fact, the controversy about the existence of the leading-edge vortex in flying insects, raised by several recent flow visualization experiments (Grodnitsky & Morozov 1992, 1993), may well be due to the low particle seeding densities in such experiments, combined with the unexpectedly small size of the vortex in the absence of a mean free-stream velocity. In smoke visualization experiments with tethered hawkmoths, Willmott *et al.* (1997) did observe a small leading-edge vortex with strong axial flow in their stereophotographs. Furthermore, their data show that this vortex rapidly increases in diameter as the forward speed increases.

(*b*) *The shape of the vortex wake*

Since the total circulation of a system must remain constant (Kelvin's circulation theorem), any change in the circulation of the bound vortex of a wing must be accompanied by the shedding of a starting or stopping vortex of equal but opposite circulation. Therefore, the mean lift force acting on flapping wings can be estimated indirectly from their vortex wake (Rayner 1979; Ellington 1980, 1984*b*). Such calculations depend strongly on the shape of the wake, which changes with time.

The initial development of the wake proceeds as follows. As the wing accelerates and decelerates smoothly during the downstroke (figure 2), the bound vortex is likely to build up and decline gradually. Calculations of the circulation of the leading-edge vortex during the downstroke support this view (Van den Berg & Ellington 1997). Such gradual changes must be accompanied by continuous shedding of starting or stopping vorticity (figure 7*a*). There must also be a spanwise gradient in circulation, with a corresponding gradient of trailing vorticity in the wake. During hovering, the circulation over the insect body and the wing base must approach zero. Therefore, the circulation will increase from the wing base to a peak somewhere along its length and then fall to zero again towards the wing tip. Indeed, the circulation of the leading-edge vortex reached a peak at about two-thirds of the wing length (Van den Berg & Ellington 1997). Such a spanwise gradient in circulation must be accompanied by a spanwise gradient in trailing vorticity, and thus the initial wake of a flapping wing must be a vortex sheet (figure 7*a*). For a hovering insect, the sheet for each wing will be a circular segment, corresponding to the swept area (Ellington 1984*b*).

A vortex sheet as described above is not stable and is not observed. It rolls up almost instantly, concentrating the vorticity into an initially wedge-shaped vortex 'ring' composed of a starting vortex, tip vortex, root vortex and stopping vortex (figure 7*b*). A likely further development of the wake is the formtion of two more circular vortex rings, as in figure 7*c*. Alternatively, the two root vortices may cancel if they are close together: their cores will entangle and break down, resulting in the single dumbbell-shaped vortex 'ring' also depicted in figure 7*c*. If a dumbbell vortex ring does form, it may subsequently either break up into two circular rings, as before, or distort into a single ring, which is the form of the vortex wake assumed by Rayner (1979). The present data indicate that the wake of the flapper is best approximated by two vortex rings (figure 6*e*). At the wing base, the downstroke vortex rings were closed off by short root vortices, which could be seen clearly in video sequences taken perpendicular to the stroke plane. The two vortex rings also drifted apart during the downstroke (figure 6), suggesting that the wake was not approaching a single vortex ring state. Brodsky (1986) described a similar 'two vortex ring wake' in visualization experiments with a cranefly; the stalked wings of this species leave a gap between wing surface and body, somewhat similar to the flapper wings.

Willmott *et al.* (1997) also found that the wake of the

hawkmoth expands to outside the swept area; however, they found no evidence of separate vortex rings per wing even under near-hovering conditions; the flow at the proximal part of the wing was unclear and no root vortices could be identified. This discrepancy is largely caused by differences in the wing's construction: the base of each hawkmoth wing lies smoothly against the body, leaving no gap, whereas in the flapper there is a gap between the wing base and the body. Hence, in the hawkmoth, the root vortices will merge with the wake of the body and the vortices of the left and right wingpair (with opposite circulation) will largely cancel out. The wake of the hawkmoth is therefore best approximated by a dumbbell-shaped vortex, as in figure 7*c*.

(*c*) *An estimate of the mean lift force during the downstroke*

Ellington (1980, 1984*b*) analysed the mean lift of hovering vortex wakes using the initial geometry of the vortex sheets, whereas Rayner (1979) took a single, rolled-up circular ring vortex as his model. These models are equivalent, because the impulse of a vortex sheet does not change during the roll up. The flapper wake is most appropriately analysed as two adjacent vortex rings, separated from each other by a distance of slightly more than their diameter (figure 6*e*). The circulation, Γ, of an isolated vortex ring can be calculated using the self-induced velocity, V, of the vortex core, the vortex ring diameter, D, and the vortex core diameter, d (e.g. Rayner 1979; Ellington 1980, 1984*b*):

$$\Gamma = \frac{2\pi DV}{\ln(8D/d) - 0.25}.$$

For simplicity, it is assumed that the two rings do not influence each other; this will lead to a small underestimate of the circulation and lift, since the ring vortices will reduce each other's speed. The velocity of the vortex core was taken as the mean velocity of the downstroke vortex: 25 cm s^{-1} (figure 6*a*). The vortex ring diameter, D, was estimated as $0.75R$, or 35 cm (figure 6*e*). The vortex core diameter, d, could not be determined accurately but is not very critical, since it appears in a logarithmic term. Rayner (1979) suggested that 0.1–$0.225D$ is a reasonable range of values which would yield estimates of Γ between 1331 and 1655 cm^2 s^{-1}. The mean lift, $\bar{L}_d$, during the downstroke can now be estimated as the impulse, I, of the wake divided by the duration, T_d, of the downstroke (rearranged formula from Rayner 1979; Ellington 1980, 1984*b*):

$$\bar{L}_d = \frac{I}{T_d} = \frac{0.25\pi\rho D^2\Gamma}{T_d},$$

where ρ is air density (1.23 kg m^{-3}) and T_d is 1.67 s. The mean lift per wing, $\bar{L}_d$, ranges from 9.4 to 11.7 mN, depending on the value for the core diameter. The mean required lift per wing is half of the weight of the hawkmoth, or 7.8 mN (see § 2*d*). Hence, the estimated mean lift during the downstroke is sufficient for weight support. In fact, it is somewhat higher than the mean required lift, which is appropriate, considering that the downstroke is thought to be stronger than the upstroke (Willmott *et al.* 1997). This estimate shows that the flow generated by the flapper corresponds well with that expected for a hovering hawkmoth. Hence, there is both qualitative (shape of the vortex wake) and quantitative agreement between experiments with the flapper and with the hawkmoth.

5. CONCLUSIONS

The air flow over the wings of a hovering model insect is quite three-dimensional. The high angles of attack generate a leading-edge vortex. The flapping motion induces a strong axial flow in this leading-edge vortex, which stabilizes it and keeps it comparatively small, but very intense. At the end of the downstroke, the wake of the flapper can be approximated by two vortex rings, one per wing. The velocity of these rings corresponds well with the predicted impulse of the wake, indicating that sufficient lift is produced for weight support. The lift-enhancing properties of the leading-edge vortex are discussed elsewhere (Van den Berg & Ellington 1997). The three-dimensional wake structure described here may well provide a new, general model for the wake of insects during hovering and slow flight.

We are grateful to Mr Richard Holder, who performed the difficult task of building and adapting the flapper with much enthusiasm, Dr Robin Wootton, who designed the flapper wing so that it accurately mimics the bending behaviour of real hawkmoth wings, and Dr Adrian Thomas who contributed to the flapper design. Dr Berend van den Berg, Dr Ali Cooper and Dr Sandy Willmott are acknowledged for comments on earlier versions of the manuscript. The project was funded by the SERC, the Hasselblad Foundation, and an EC Human Capital and Mobility grant.

REFERENCES

Brodsky, A. K. 1986 Flight of insects with high wingbeat frequencies. *Ent. Obozr.* **65**, 269–279. (In Russian.)

Brodsky, A. K. 1991 Vortex formation in the tethered flight of the peacock butterfly *Inachis io* L. (Lepidoptera, Nymphalidae) and some aspects of insect flight evolution. *J. exp. Biol.* **161**, 77–95.

Brodsky, A. K. & Grodnitsky, D. L. 1985 Aerodynamics of fixed flight of *Thymelicus lineola* Ochs. (Lepidoptera, Hesperiidae). *Entomological Review* **64**, 60–69. (Originally published in Russian in *Ent. Obozr.* **3**, 484–492.)

Délery, J. M. 1994 Aspects of vortex breakdown. *Prog. Aerospace Sci.* **30**, 1–59.

Dickinson, M. H. 1994 The effects of wing rotation on unsteady aerodynamic performance at low Reynolds numbers. *J. exp. Biol.* **192**, 179–206.

Dickinson, M. H. & Götz, K. G. 1993 Unsteady aerodynamic performance of model wings at low Reynolds numbers. *J. exp. Biol.* **174**, 45–64.

Ellington, C. P. 1980 Wing mechanics and take-off preparation of *Thrips* (Thysanoptera). *J. exp. Biol.* **85**, 129–136.

Ellington, C. P. 1984*a* The aerodynamics of hovering insect flight. IV. Aerodynamic mechanisms. *Phil. Trans. R. Soc. Lond.* B **305**, 79–113.

Ellington, C. P. 1984*b* The aerodynamics of hovering insect flight. V. A vortex theory. *Phil. Trans. R. Soc. Lond.* B **305**, 115–144.

Ellington, C. P. 1995 Unsteady aerodynamics of insect flight. In *Biological fluid dynamics* (ed. C. P. Ellington & T. J. Pedley), *Symp. Soc. exp. Biol.* **49**, 109–129.

Grodnitsky, D. L. & Morozov, P. P. 1992 Flow visualization experiments on tethered flying green lacewings *Chrysopa dasyptera*. *J. exp. Biol.* **169**, 143–163.

Grodnitsky, D. L. & Morozov, P. P. 1993 Vortex formation during tethered flight of functionally and morphologically two-winged insects, including evolutionary considerations on insect flight. *J. exp. Biol.* **182**, 11–40.

Gursul, I., Lusseyran, D. & Rockwell, D. 1990 On interpretation of flow visualization of unsteady shear flows. *Experiments in fluids* **9**, 257–266.

Maxworthy, T. 1979 Experiments on the Weis-Fogh mechanism of lift generation by insects in hovering flight. Part 1. Dynamics of the 'fling'. *J. Fluid Mech.* **93**, 47–63.

Nachtigall, W. 1979 Rasche Richtungsänderungen und Torsionen schwingender Fliegenflügel und Hypothesen über zugeordnete instationäre Strömungseffekte. *J. comp. Physiol.* **133**, 351–355.

Rayner, J. M. V. 1979 A vortex theory of animal flight. Part 1. The vortex wake of a hovering animal. *J. Fluid Mech.* **91**, 697–730.

Rayner, J. M. V. & Thomas, A. L. R. 1991 On the vortex wake of an animal flying in a confined volume. *Phil. Trans. R. Soc. Lond.* B **334**, 107–117.

Saharon, D. & Luttges, M. 1987 Three-dimensional flow produced by a pitching–plunging model dragonfly wing. *Amer. Inst. of Aeronautics and Astronautics* **121**, 1–17.

Saharon, D. & Luttges, M. W. 1988 Visualization of unsteady separated flow produced by mechanically driven dragonfly wing kinematics model. *Amer. Inst. of Aeronautics and Astronautics* **569**, 1–23.

Savage, S. B., Newman, B. G. & Wong, D. T.-M. 1979 The role of vortices and unsteady effects during the hovering flight of dragonflies. *J. exp. Biol.* **83**, 59–77.

Spedding, G. R. and Maxworthy, T. 1986 The generation of circulation and lift in a rigid two-dimensional fling. *J. Fluid Mech.* **165**, 247–272.

Sunada, S., Kawachi, K., Watanabe, I. and Azuma, A. 1993 Fundamental analysis of three-dimensional 'near fling'. *J. exp. Biol.* **183**, 217–248.

Van den Berg, C. & Ellington, C. P. (1997) The three-dimensional leading-edge vortex of a 'hovering' model hawkmoth. *Phil. Trans. R. Soc. Lond.* B **352**, 329–340.

Weis–Fogh, T. 1973 Quick estimates of flight fitness in hovering animals, including novel mechanisms for lift production. *J. exp. Biol.* **59**, 169–230.

Willmott, A. P. 1995 *The mechanics of hawkmoth flight*. Ph.D. thesis, University of Cambridge.

Willmott, A. P., Ellington, C. P. & Thomas, A. L. R. 1997 Flow visualization and unsteady aerodynamic mechanisms in the flight of the hawkmoth *Manduca sexta*. *Phil. Trans. R. Soc. Lond.* B **352**, 303–316.

Wu, J. Z., Vakili, A. D. & Wu, J. M. 1991 Review of the physics of enhancing vortex lift by unsteady excitation. *Prog. Aerospace Sci.* **28**, 73–131.

Received 9 May 1996; accepted 22 August 1996

PHILOSOPHICAL TRANSACTIONS OF THE ROYAL SOCIETY B BIOLOGICAL SCIENCES